Langmuir

Article

pubs.acs.org/Langmuir

Improved Photoelectrochemical Water Oxidation by the $WO_3/CuWO_4$ Composite with a Manganese Phosphate Electrocatalyst

Ki Min Nam,[†] Eun Ah Cheon,[†] Won Jung Shin,[†] and Allen J. Bard*[,‡]

[†]Department of Chemistry, Mokpo National University, Jeonnam 534-729, Korea

[‡]Center for Electrochemistry, Department of Chemistry, The University of Texas at Austin, Austin, Texas 78712, United States

Supporting Information

ABSTRACT: We describe a composite of the n-type semiconductors for the photoelectrochemical oxygen evolution reaction (OER). A simple drop-casting technique of mixed precursors and a one-step annealing process were used in the synthesis of the $WO_3/CuWO_4$ composite. The composite showed improved photocurrent for water oxidation compared to either of the two compounds individually. We discuss possible electron−hole separation mechanisms in two semiconductors comprising a primary photon-absorbing semiconductor of $CuWO_4$ with a secondary semiconductor of WO_3. When the $WO_3/CuWO_4$ composite is simultaneously irradiated, the photogenerated hole from the WO_3 valence band transfers to $CuWO_4$, which results in an enhanced charge separation of $CuWO_4$. Furthermore, the OER catalytic activity of manganese phosphate (MnPO) was compared to manganese oxide nanoparticles (Mn_2O_3) by electrochemical measurements, showing that the manganese phosphate was more efficient for the OER reaction. To investigate the effect of catalysts on semiconductors, manganese phosphate was deposited on the $WO_3/CuWO_4$ composite. The result demonstrates the promise of manganese phosphate for improving the photocurrent as well as the stability of the $WO_3/CuWO_4$ composite.

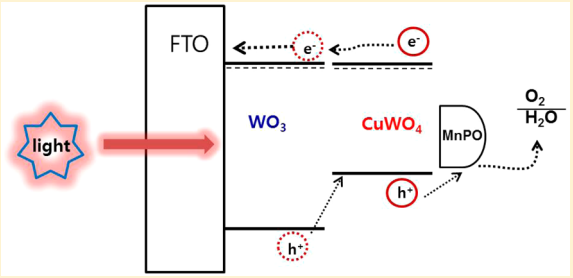

1. INTRODUCTION

Metal oxide n-type semiconductors have been extensively studied as photoanodes for solar water oxidation because of their chemical stability and relatively low cost.[1−3] However, they have limitations including poor visible light absorption, significant electron−hole recombination, and slow surface water oxidation kinetics.[4,5] Various strategies such as doping, morphology control, and adjusting the surface structure have been developed to try to address these problems. Furthermore, the fabrication of a composite structure of two semiconductors has suggested the advancement of photoelectrochemical (PEC) water splitting.[6−8] The composite not only expands the spectral range of light absorption but also promotes charge separation, thus significantly enhancing the energy efficiency.[9,10] For example, composite electrodes of $WO_3/BiVO_4$[11−13] have been extensively studied as promising PEC electrodes due to more efficient charge separation in the composite, with $BiVO_4$ as the primary light absorber and WO_3 presumably acting as an electron conductor. Although the advantages of pairing semiconductors are now widely appreciated, the origins of electron−hole separation are still far from being understood.

$CuWO_4$ is an n-type semiconductor and has been identified as a photoanode for water oxidation.[14,15] Compared to WO_3, $CuWO_4$ is more stable against photocorrosion in aqueous solution, and this semiconductor can harvest visible light at wavelengths of up to 540 nm (~2.3 eV bandgap) with appropriate conduction and valence band edges.[16] However, the slow carrier mobility in the bulk and fast recombination at the surface contributes to the poor overall efficiency for PEC water oxidation at $CuWO_4$.

In this paper, we discuss the spontaneous formation of $WO_3/CuWO_4$ composite structures and possible electron−hole separation mechanisms for the improvement of the PEC water oxidation efficiency. The $WO_3/CuWO_4$ composites typically comprise a primary photon-absorbing semiconductor of $CuWO_4$ with a secondary semiconductor of WO_3 that may play a number of assisting roles, which are constructed to improve the processes of electron−hole separation and charge transport through the composite. Further, the experiments of the OER (water oxidation) catalytic activity of a manganese phosphate were undertaken. The composite structure with the manganese phosphate (MnPO) electrocatalyst helps to overcome the kinetic limitations of water oxidation at the $CuWO_4$ surface.

2. EXPERIMENTAL SECTION

Materials. Fluorine-doped tin oxide (FTO, TEC 15, WY-GMS)-coated glass was used as the substrate for the thin film electrodes. $(NH_4)_6H_2W_{12}O_{40}\cdot xH_2O$ (≥99.0%, Sigma-Aldrich), $Cu(NO_3)_2\cdot 2H_2O$ (99%, Sigma-Aldrich), $MnCl_2\cdot 2H_2O$ (99%, Sigma-Aldrich), and $Mn(acac)_2$ (Sigma-Aldrich) were used as received as the metal precursor salts. In addition, D-(+)-glucose (99.5%, Sigma-Aldrich),

Received: May 15, 2015
Revised: August 21, 2015
Published: September 15, 2015

DOI: 10.1021/acs.langmuir.5b01780
Langmuir 2015, 31, 10897−10903

benzylalcohol (99.0%, JUNSEI), HEPES (2,4-(2-hydroxyethyl)-1-piperazinyl) ethane-sulfonic acid, Sigma-Aldrich), Na_2SO_4, Na_2HPO_4, NaH_2PO_4, ethylene glycol (99.0%), acetone (99.0%), and ethanol (99.5%) were purchased from Daejung Chemicals (Korea). Deionized water was used as the solvent in electrochemical experiments.

Preparation of Thin Film Electrodes. FTO substrates were first cleaned in deionized water and ethanol and then sonicated in ethanol for at least 1 h. A drop-casting technique was used to create the thin film electrodes. Here 200 μL of a 20 mM precursor solution in ethylene glycol containing either the W precursor or the mixed (Cu and W) precursor was dropped onto the FTO substrate (~1.5 cm × 2 cm) with a drying step at 120 °C in air. To create samples of various ratios, the precursor Cu/W ratio was varied from 1/1 ($CuWO_4$) to 0/2 (WO_3). The prepared films were annealed at 550 °C for 3 h (with a 3 h ramp time) in air to form the metal oxide materials (WO_3, $CuWO_4$, and $WO_3/CuWO_4$ composites).

Preparation of the Manganese Phosphate (MnPO) Electrocatalyst. The manganese phosphate (MnPO) complex was prepared by adding 0.1 M NaH_2PO_4 in HEPES (2 mM) to a 0.1 M $MnCl_2 \cdot 4H_2O$ solution at 100 °C for 3 h in air, and the resulting white reaction mixture was cooled to room temperature. The residue was washed with ethanol to provide white manganese phosphate.

Preparation of Mn_2O_3. A slurry of $Mn(acac)_2$ (50 mg) in benzylalcohol (5.0 g) with a carbon sphere template[17] (50 mg) was heated to 180 °C under an argon atmosphere. The reaction mixture was maintained at this temperature for 3 h, and the resulting dark-brown reaction mixture was cooled to room temperature. The residue was washed with ethanol to provide dark-brown MnO/carbon powders. MnO/carbon powders were loaded in an alumina boat in a box furnace and were annealed at 500 °C for 3 h under an atmospheric pressure of air, which shows a phase transition of MnO to hollow Mn_2O_3.

Electrochemical Characterization of Thin Film Electrodes. Electrochemcial characterization was performed in a specially designed cell in a three-electrode configuration with the thin film as the working electrode, a Pt wire counter electrode, and a Ag/AgCl reference electrode. The actual geometric area of the working electrode with a 0.28 cm^2 geometric area was exposed in the electrolyte (0.1 M phosphate buffer, pH 7). The 150 W xenon lamp (ABET Technologies) was used as the light source in the PEC characterization. Chopped light linear sweep voltammetry (LSV) was used to obtain the photocurrent responses using a DY2321 potentiostat (Digi-Ivy). The PEC measurements were performed in aqueous solutions of 0.1 M Na_2SO_4 with a phosphate buffer (pH 7) for water oxidation. In all tests, the intensity of the lamp on the sample was measured to be 100 mW/cm^2 using a Si solar cell (AIST). A 425 nm long-pass filter was used to cut the UV portion of the spectrum and to provide only visible light illumination. A monochromator (ORIEL) was used to obtain action spectra of the photoresponse as a function of wavelength.

Each catalyst (MnPO and hollow Mn_2O_3) with Nafion solution was drop-cast on the FTO substrate. The electrocatalyst films were used as working electrodes with a 0.28 cm^2 geometric area exposed to electrolyte solution (0.1 M phosphate buffer, pH 7). The electrode was first cycled five times by cyclic voltammetry until a stable cyclic voltammogram developed before measuring the linear sweep voltammetric behavior.

Materials Characterization of Thin Film Electrodes. UV−vis absorption spectra were acquired with a Lambda 3B spectrophotometer (PerkinElmer) for wavelengths from 300 to 900 nm. The thin film electrodes were characterized by scanning electron microscopy (SEM, Philips XL30SFEG operated at 10 and 30 kV). The X-ray diffraction data was measured using Cu Kα radiation at 40 kV and 100 mA (Rigaku, Dmax-RB diffractometer).

3. RESULTS AND DISCUSSION

PEC at the $WO_3/CuWO_4$ Composite. To investigate the effect of the Cu−W−O composition, thin film electrodes were prepared by drop casting the precursor solutions on an FTO substrate. For the WO_3 (band gap: 2.7 eV), $CuWO_4$ (band gap: 2.3 eV), and $WO_3/CuWO_4$ composites, the atomic ratio of the Cu/W precursor was varied from 1/1 ($CuWO_4$) to 0/2 (WO_3) (Scheme 1).

Scheme 1. Prepared Thin Film Electrodes with Different Ratios of Cu and W Components

Cu / W						
(1) 1 / 1 ($CuWO_4$)	(2) 0.95 / 1.05	(3) 0.9 / 1.1	(4) 0.85 / 1.15	(5) 0.8 / 1.2	(6) 0.75 / 1.25	(7) 0.7 / 1.3
(8) 0.65 / 1.35	(9) 0.6 / 1.4	(10) 0.55 / 1.45	(11) 0.5 / 1.50	(12) 0.45 / 1.55	(13) 0.4 / 1.6	(14) 0.35 / 1.65
(15) 0.3 / 1.7	(16) 0.25 / 1.75	(17) 0.2 / 1.8	(18) 0.15 / 1.85	(19) 0.1 / 1.9	(20) 0.05 / 1.95	(21) 0 / 2 (WO_3)

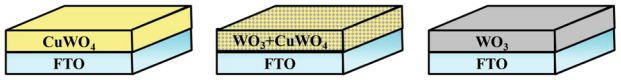

(1) (2) – (20) (21)

After drop casting, the prepared films were annealed at 550 °C for 3 h in air to form thin film electrodes. Figure 1 shows the scanning electron microscopy (SEM) image of $CuWO_4$ and WO_3 with continuous morphology with small grain sizes below 200 nm. The X-ray diffraction (XRD) peaks have been indexed to the monoclinic structure of WO_3 and the triclinic structure of $CuWO_4$ (Figure 2). Typically, the ratio in between (from 0.95/1.05 to 0.05/1.95) resulted in various $WO_3/CuWO_4$ composite structures (Scheme 1). The scanning electron microscopy (SEM) image showed continuous morphology with different grain sizes of the $WO_3/CuWO_4$ composite (Figure 1c).

The composite structure of $WO_3/CuWO_4$ was further identified by SEM and energy-dispersive X-ray spectroscopy (EDS) measurements (Figure S1 in the Supporting Information). From the EDS mapping images, the WO_3 and $CuWO_4$ sizes were estimated to be ~40 and ~100 nm, respectively. The crystallite sizes were additionally determined by XRD using the Debye−Scherrer equation[18] and are 40 nm (WO_3) and 80 nm ($CuWO_4$) (Figures 2 and S2), which matched the EDS images well. Most WO_3 particles initially crystallize on the bottom layer (Figure S1e).

The PEC performance of the WO_3, $CuWO_4$, and $WO_3/CuWO_4$ composite (Cu/W = 0.4/1.6, sample 13 in Scheme 1) electrodes was studied using linear sweep voltammetry (LSV) in 0.1 M Na_2SO_4 (pH 7, 0.1 M phosphate-buffered). The LSV was conducted from −0.2 to +0.8 V vs Ag/AgCl at a scan rate of 20 mV/s with chopped light under UV−visible irradiation (Figure 3).

All three electrodes successfully generated anodic photocurrents, which confirmed the n-type characteristics of the thin film electrodes. The WO_3 and $CuWO_4$ electrodes had approximately the same photocurrent, and the $WO_3/CuWO_4$ composite electrode attained at least a 2-fold higher photocurrent than the $CuWO_4$ for water oxidation. To investigate the optimized ratio of W and Cu, we created film electrodes of Cu/W ranging from 0.95/1.05 to 0.05/1.95. Figure 4 shows the net photocurrent at 0.6 V vs Ag/AgCl for water oxidation as a function of W and Cu ratios under UV−visible and visible (>425 nm) irradiation to illustrate how the composite affects

DOI: 10.1021/acs.langmuir.5b01780
Langmuir 2015, 31, 10897−10903

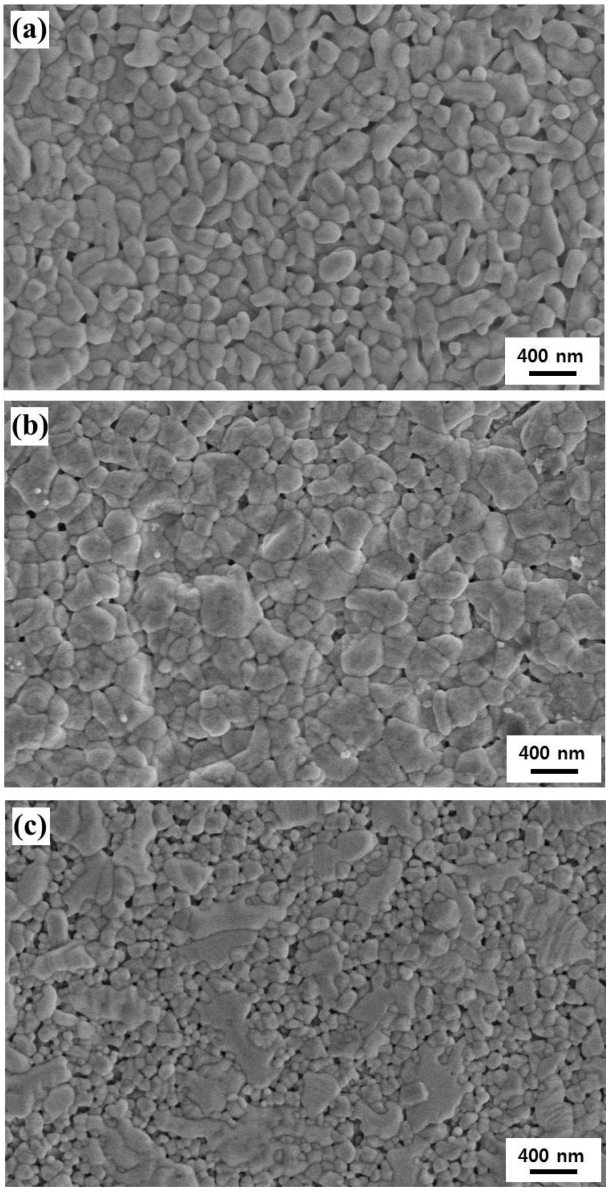

Figure 1. SEM images of thin film electrodes: (a) $CuWO_4$, (b) WO_3, and (c) $WO_3/CuWO_4$ composites (Cu/W = 0.4/1.6, sample 13 in Scheme 1).

water oxidation. From the net photocurrent in Figure 4, we see that a maximum photocurrent response occurred between 0.8/1.2 and 0.2/1.8 ratios of Cu/W. Note that the composite shows an enhanced photocurrent under full UV−visible irradiation, but the visible region response is similar to that for the $CuWO_4$ film alone (Figure 4).

Proposed Mechanism. We observe that $CuWO_4$ has approximately the same photocurrent for water oxidation compared to WO_3 but that a composite of $WO_3/CuWO_4$ produces a higher photocurrent for water oxidation than either of the two compounds individually. On the basis of the SEM image (Figure S1e), a composite structure has mostly an FTO/WO_3/$CuWO_4$ arrangement. In addition, when we make a layered structure such as FTO/WO_3/$CuWO_4$, this shows enhanced PEC activity (Figure S3). As suggested by the diagrams of the two materials shown in Scheme 2, we propose that improved electron−hole separation leads to a higher photocurrent. This involves two effects: transfer of a hole from

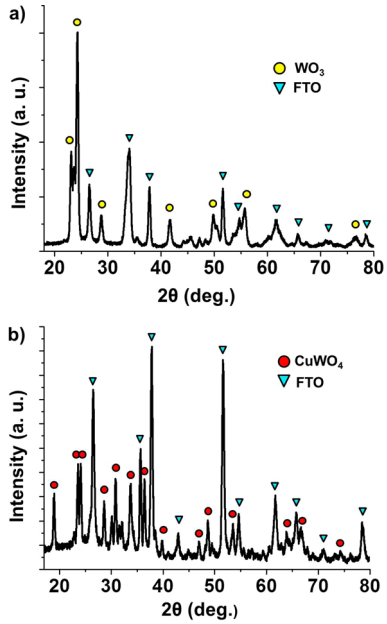

Figure 2. XRD patterns of (a) WO_3 and (b) $CuWO_4$ electrodes on the FTO substrate.

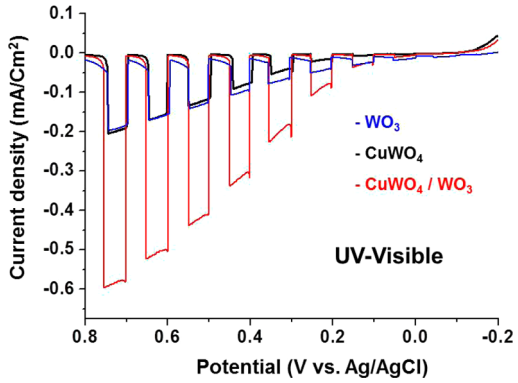

Figure 3. LSVs of WO_3, $CuWO_4$, and $WO_3/CuWO_4$ electrodes in phosphate buffer (pH 7) under UV−visible illumination. Scan rate: 20 mV/s. Light intensity: 100 mW/cm^2.

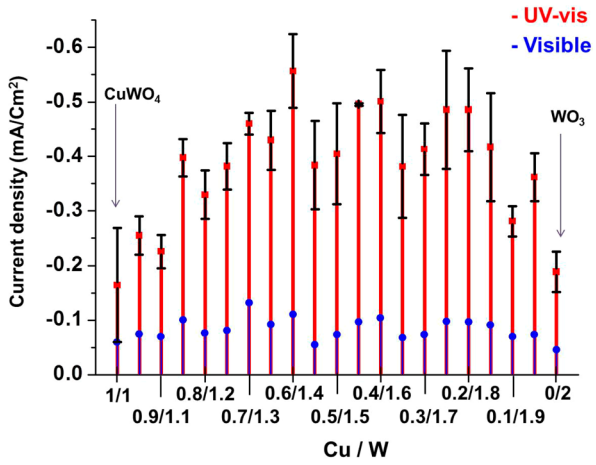

Figure 4. Photocurrent with different molar ratios between Cu and W at an applied potential of 0.6 V versus Ag/AgCl in phosphate buffer (pH 7). Light intensity: 100 mW/cm^2.

DOI: 10.1021/acs.langmuir.5b01780
Langmuir 2015, 31, 10897−10903

Scheme 2. Photogenerated Electron−Hole Pathways between Two Semiconductors (WO_3 and $CuWO_4$)[a]

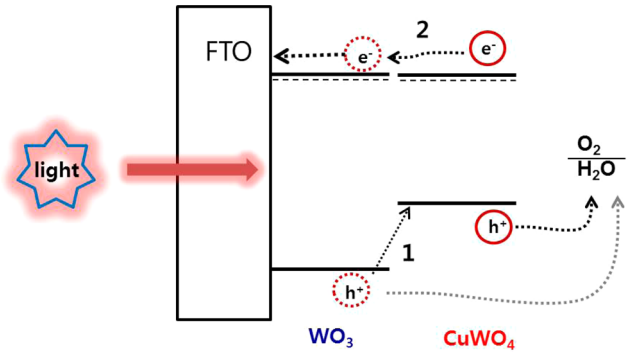

[a](1) Transfer of a hole from the valence band of WO_3 to that of $CuWO_4$. (2) Electron transfer from the conduction band of $CuWO_4$ to that of WO_3.

the valence band of WO_3 to that of $CuWO_4$ and electron transfer from $CuWO_4$ to that of WO_3. The latter is equivalent to sensitization by the smaller band gap semiconductor in an analogous way to dye sensitization of a larger band gap semiconductor. For the elucidation of the mechanism, we investigated the distribution of the photocurrent depending on the wavelength when it formed into a $WO_3/CuWO_4$ composite. Chopped light with the monochromator adjusted to obtain photocurrents at wavelengths with 10 nm intervals was employed. The band gaps were determined from the wavelengths for the onset of the photocurrent (Figure 5).

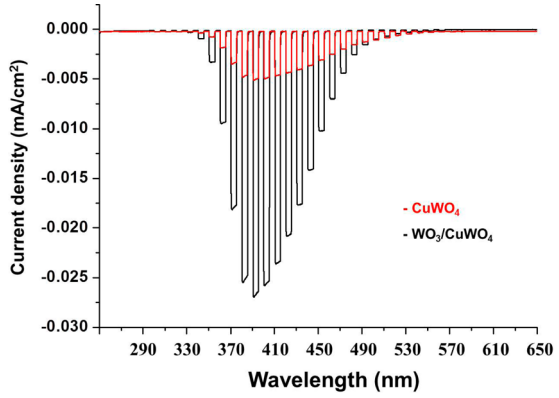

Figure 5. Action spectrum of $CuWO_4$ and $WO_3/CuWO_4$ composite electrodes at an applied potential of 0.6 V versus Ag/AgCl in phosphate buffer (pH 7).

The $WO_3/CuWO_4$ composite shows the same onset wavelength as for $CuWO_4$ (540 nm, 2.3 eV), which indicates the band gap of $CuWO_4$. Typically, the $WO_3/CuWO_4$ composite shows a larger photocurrent until 490 nm compared to $CuWO_4$ but essentially it shows the same photocurrent above 490 nm. The onset wavelength of WO_3 is 490 nm (Figure S4), suggesting an important role in the water oxidation process. $CuWO_4$ and WO_3 have the same conduction band potential, but the valence band of WO_3 is more positive than that of $CuWO_4$.[19,20] Because the enhanced photocurrent of the composite is not observed above 490 nm in the action spectrum (Figure 5), we attribute the enhancement from WO_3 by pathway 1 in Scheme 2. When the $WO_3/CuWO_4$ composite is simultaneously irradiated, the photogenerated hole from the WO_3 valence band transfers to $CuWO_4$, which results in an enhanced charge separation of $CuWO_4$. And the photogenerated electron can freely transfer through either way because $CuWO_4$ and WO_3 have the same conduction band potential as determined by onset potentials. Photocurrent onsets are observed at the same potential of around −0.15 V (vs Ag/AgCl) for both WO_3 and $CuWO_4$ (Figure 3), which matches well with the literature.[19,20] This value can be taken to approximate the conduction band edge of WO_3 and $CuWO_4$. The band gap can also be estimated from the onset of UV−visible absorbance (Figure S5). From the absorbance data, the $CuWO_4$ and the $WO_3/CuWO_4$ composite samples showed indirect transitions with band gaps of ∼2.3 eV. The band gap obtained from the absorbance agrees well with the action spectrum data, and the onset wavelength of $CuWO_4$ is essentially the same.

Manganese Phosphate Electrocatalyst. The photocurrent for the OER was increased even more by the addition of a manganese phosphate electrocatalyst to the composite. The water oxidation catalyst of photosynthesis composed of earth-abundant elements such as Mn and Ca in the form of a cubical $CaMn_4O_5$ cluster catalyzes water oxidation under neutral conditions with an extremely low overpotential value.[21] The unique capabilities of the natural system have inspired the design of Mn-based catalysts for water oxidation.[22] Metal phosphate is an interesting material as a water oxidation catalyst, which shows highly active catalytic properties under neutral conditions.[23,24] However, manganese phosphate has not been fully characterized as an electrocatalyst associated with a photocatalyst. The manganese phosphate complex was prepared by adding 0.1 M NaH_2PO_4 in HEPES (2 mM) buffer to a 0.1 M $MnCl_2{\cdot}4H_2O$ solution at 100 °C for 3 h in air. Figure 6 shows the SEM images of manganese phosphate with

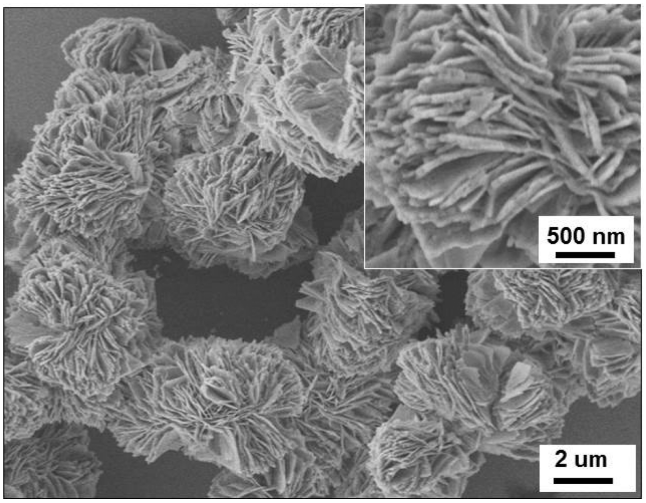

Figure 6. SEM image of manganese phosphate (MnPO) nanoplates.

an aggregated thin-layer morphology with a regular thickness of ∼30 nm (Figure 6, inset). The XRD patterns of the manganese phosphate are shown in Figure S6 in the Supporting Information. The diffraction peaks have been indexed to the monoclinic $Mn_5(PO_3(OH))_2(PO_4)_2(H_2O)_4$ (MnPO, PDF no. 86-1521).

To investigate the catalytic property of MnPO, the well-known manganese oxide (Mn_2O_3) catalyst was prepared for a comparison. Mn_2O_3 was synthesized by a reported method

DOI: 10.1021/acs.langmuir.5b01780
Langmuir 2015, 31, 10897−10903

with some modification.[17] Note that the Mn_2O_3 structure has been known as the best water oxidation catalyst among the manganese oxide structures (MnO, Mn_3O_4, Mn_2O_3, and MnO_2).[22] The OER catalytic activity of the MnPO and Mn_2O_3 nanoparticles drop cast on FTO were obtained by electrochemical measurement in 0.1 M phosphate buffer (pH 7) using a three-electrode cell setup. Figure 7 shows oxidation

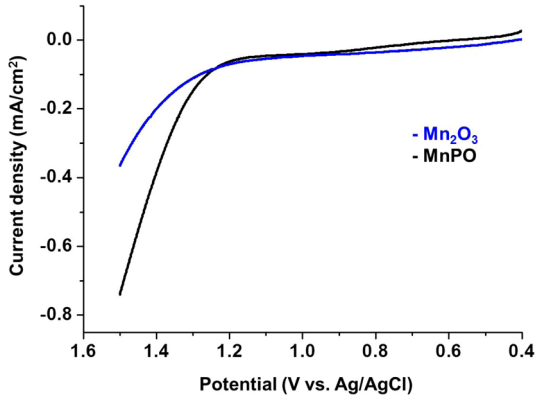

Figure 7. LSVs of manganese phosphate (MnPO) and Mn_2O_3 in 0.1 M phosphate buffer (pH 7). Scan rate: 20 mV/s. The current density area was taken as the projected area of the electrode.

currents of the MnPO and Mn_2O_3 nanoparticles. The oxygen evolution ability of MnPO was higher than that of pure Mn_2O_3. The current of the MnPO catalyst was 0.72 mA/cm^2, whereas Mn_2O_3 was below 0.35 mA/cm^2 at an overpotential of 850 mV. Our result shows that MnPO is more efficient for water oxidation than the manganese oxides. For the qualitative detection of O_2 with the MnPO electrode, chronoamperometry was carried out at 1.4 V vs Ag/AgCl for 30 min. Bubbles, assumed to be O_2, were observed on the surface of the MnPO electrode (Figure S7).

The electrocatalysts associated with the semiconductor photoelectrode can improve the PEC water oxidation. Intensive attention is currently focused on the discovery of good cocatalysts for PEC-OER, but the best electrocatalysts do not always perform equally well when integrated into a PEC-OER system.[25,26] The interface between the semiconductor and the catalyst may play a role. To investigate the effect of this catalyst on the composite structures, MnPO and Mn_2O_3 electrocatalysts were deposited on the WO_3/$CuWO_4$ composite. The PEC performance of the WO_3/$CuWO_4$/MnPO and WO_3/$CuWO_4$ composite (Cu/W = 0.8/1.2, 5 sample in Scheme 1) electrodes were studied using LSV in 0.1 M Na_2SO_4 (pH 7, 0.1 M phosphate-buffered) under UV−visible irradiation (Figure 8a). The WO_3/$CuWO_4$/MnPO composite electrode attained at least a 1.5-fold higher photocurrent than WO_3/$CuWO_4$ for water oxidation (at +0.5 V vs Ag/AgCl). However, Mn_2O_3 does not show any catalytic activity on WO_3/$CuWO_4$.

To assess the stability of the composite electrodes over time, chronoamperometry was carried out at 0.4 V versus Ag/AgCl under UV−visible irradiation (Figure 8b). The first photocurrent−time profile of WO_3/$CuWO_4$ was obtained over 20 min (black line in Figure 8b) and then deposited the MnPO on this electrode to make WO_3/$CuWO_4$/MnPO for the following experiment. The photocurrent using WO_3/$CuWO_4$/MnPO showed high photoelectrochemical stability (red line in Figure 8b), while WO_3/$CuWO_4$ alone under the same condition decayed rapidly, dropping by 20% over 20 min, indicating

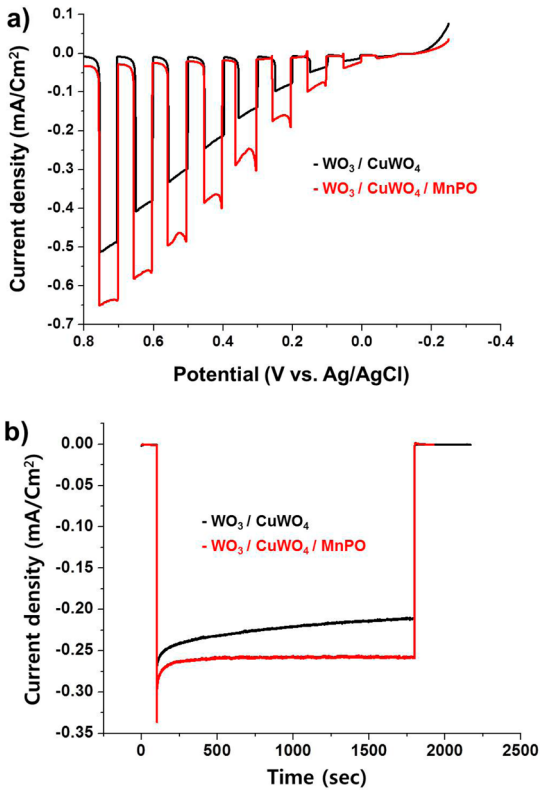

Figure 8. (a) LSVs of WO_3/$CuWO_4$ and WO_3/$CuWO_4$/MnPO electrodes in phosphate buffer (pH 7) under UV−visible illumination. Scan rate: 20 mV/s. Light intensity: 100 mW/cm^2. (b) Current−time response curve of the WO_3/$CuWO_4$ and WO_3/$CuWO_4$/MnPO electrodes at an applied potential of 0.4 V versus Ag/AgCl in phosphate buffer (pH 7).

enhanced stability by the MnPO electrocatalysts. The instability of the WO_3/$CuWO_4$ composite is attributed to the interaction between the electrolyte (phosphate and/or sulfate) anion and the electrode surface (WO_3 and $CuWO_4$) under neutral conditions.[20,27] When a phosphate solution was used, oxygen evolution and the formation of peroxo species were the two major photo-oxidation reactions on the WO_3 surface.[28] The accumulation of peroxo species on the WO_3 surface is known to cause a gradual photocurrent decay. When an electrocatalyst such as Co-Pi is used on a WO_3 electrode, the formation of surface-bound peroxo species was suppressed with improved stability.[29] Similarly, the presence of the MnPO electrocatalyst may suppress the formation of surface-bound peroxo species, preventing the photochemical deactivation of WO_3 and $CuWO_4$. However, it is not clear whether the presence of an MnPO catalyst inhibits the formation of the surface peroxo species or produces other intermediate species, so a more quantitative analysis is necessary. The activity, however, is not retained for a long time. The MnPO catalyst is easily detached when O_2 is generated on the MnPO surface because we just drop cast MnPO catalysts on the semiconductor. We found similar phenomena when we used drop-casting using a well-known OER catalyst of Co_3O_4 nanoparticles.

MnPO is a promising cocatalyst because it does not absorb in the visible spectrum during the PEC experiment. When the MnPO catalyst was deposited on other semiconductors such as $BiVO_4$ and Fe_2O_3, the photocurrent also showed enhanced PEC efficiency (Figure S8). We are currently investigating the

DOI: 10.1021/acs.langmuir.5b01780
Langmuir 2015, 31, 10897−10903

detailed mechanisms of MnPO on a semiconductor for a better understanding of PEC water oxidation reactions.

A long-term stability test of the $WO_3/CuWO_4$ composite was carried under UV−visible irradiation in phosphate buffer (pH7). Although the $WO_3/CuWO_4$ composite showed an initial drop in photocurrent (Figure S9b), the photocurrent stabilized at a steady-state value of 0.2 mA/cm^2 (Figure S9b). The $WO_3/CuWO_4$ composite is chemically stable during PEC water oxidation. Because no other oxidation reactions are possible in phosphate buffer, the current flow is predominantly from the OER.

4. CONCLUSIONS

$WO_3/CuWO_4$ composites were synthesized by a simple drop-casting technique of mixed precursors and a one-step annealing process. We discussed the spontaneous formation of $WO_3/CuWO_4$ composite structures and possible electron−hole separation mechanisms for the improvement of PEC water oxidation efficiency. The $WO_3/CuWO_4$ composite showed improved photocurrent over either of the two compounds individually. The $WO_3/CuWO_4$ composite, typically comprising a primary photon-absorbing semiconductor of $CuWO_4$ with a secondary semiconductor of WO_3 that may play a number of assisting roles, is constructed to improve the processes of charge transport through the composite. The water oxidation catalytic activity of the manganese phosphate (MnPO) compared to that of the manganese oxide nanoparticle (Mn_2O_3) was investigated by electrochemical measurements. The OER at manganese phosphate was higher than manganese oxide. Furthermore, the manganese phosphate electrocatalyst was deposited on the $WO_3/CuWO_4$ composite to investigate the effect of catalysts on the semiconductor. The result demonstrates the promise of manganese phosphate for improving the photocurrent as well as the stability of the $WO_3/CuWO_4$ composite.

■ ASSOCIATED CONTENT

Supporting Information

The Supporting Information is available free of charge on the ACS Publications website at DOI: 10.1021/acs.langmuir.5b01780.

Details of the synthesis procedure, SEM, XRD, UV−vis, and action spectrum results of composite electrodes (PDF)

■ AUTHOR INFORMATION

Corresponding Author

*E-mail: ajbard@mail.utexas.edu. E-mail: namkimin.chem@gmail.com (K.M.N.).

Notes

The authors declare no competing financial interest.

■ ACKNOWLEDGMENTS

We acknowledge the Division of Chemical Sciences, Geosciences, and Biosciences Office of Basic Energy Sciences of the U.S. Department of Energy SISGR (DE-FG02-09ER16119) and the Robert A. Welch Foundation (F-0021). This work was also supported by the Basic Science Research Program through the National Research Foundation of Korea (NRF) funded by the Ministry of Science, ICT & Future Planning (NRF-2015R1C1A1A02037373). We thank K. H. Oh, M. Park, and K. S. Park for the sample analysis.

■ REFERENCES

(1) Bard, A. J.; Fox, M. A. Artificial Photosynthesis: Solar Splitting of Water to Hydrogen and Oxygen. *Acc. Chem. Res.* **1995**, *28*, 141−145.
(2) Kudo, A.; Miseki, Y. Heterogeneous Photocatalyst Materials for Water Splitting. *Chem. Soc. Rev.* **2009**, *38* (1), 253−278.
(3) Osterloh, F. E. Inorganic Nanostructures for Photoelectrochemical and Photocatalytic Water Splitting. *Chem. Soc. Rev.* **2013**, *42*, 2294−2320.
(4) Park, Y.; McDonald, K. J.; Choi, K.-S. Progress in Bismuth Vanadate Photoanodes for Use in Solar Water Oxidation. *Chem. Soc. Rev.* **2013**, *42*, 2321−2337.
(5) Swierk, J. R.; Mallouk, T. E. Design and Development of Photoanodes for Water-splitting Dye-sensitized Photoelectrochemical Cells. *Chem. Soc. Rev.* **2013**, *42*, 2357−2387.
(6) Nozik, A. J. Photoelectrochemistry: Applications to Solar Energy Conversion. *Annu. Rev. Phys. Chem.* **1978**, *29*, 189−222.
(7) Pilli, S. K.; Deutsch, T. G.; Furtak, T. E.; Brown, L. D.; Turner, J. A.; Herring, A. M. BiVO(4)/CuWO(4) Heterojunction Photoanodes for Efficient Solar Driven Water Oxidation. *Phys. Chem. Chem. Phys.* **2013**, *15*, 3273−3278.
(8) Zhong, D. K.; Choi, S.; Gamelin, D. R. Near-complete Suppression of Surface Recombination in Solar Photoelectrolysis by "Co-Pi" Catalyst-modified W:BiVO4. *J. Am. Chem. Soc.* **2011**, *133* (45), 18370−18377.
(9) Leonard, K. C.; Nam, K. M.; Lee, H. C.; Kang, S. H.; Park, H. S.; Bard, A. J. $ZnWO_4/WO_3$ Composite for Improving Photoelectrochemical Water Oxidation. *J. Phys. Chem. C* **2013**, *117* (31), 15901−15910.
(10) Nam, K. M.; Park, H. S.; Lee, H. S.; Meekins, B. H.; Leonard, K. C.; Bard, A. J. Compositional Screening of the Pb−Bi−Mo−O System. Spontaneous Formation of a Composite of *p*-$PbMoO_4$ and *n*-Bi_2O_3 with Improved Photoelectrochemical Efficiency and Stability. *J. Phys. Chem. Lett.* **2013**, *4* (16), 2707−2710.
(11) Su, J.; Guo, L.; Bao, N.; Grimes, C. A. Nanostructured $WO_3/BiVO_4$ Heterojunction Films for Efficient Photoelectrochemical Water Splitting. *Nano Lett.* **2011**, *11* (5), 1928−1933.
(12) Hong, S. J.; Lee, S.; Jang, J. S.; Lee, J. S. Heterojunction $BiVO_4/WO_3$ electrodes for enhanced photoactivity of water oxidation. *Energy Environ. Sci.* **2011**, *4*, 1781−1787.
(13) Kim, T. W.; Choi, K.-S. Nanoporous $BiVO_4$ Photoanodes with Dual-Layer Oxygen Evolution Catalysts for Solar Water Splitting. *Science* **2014**, *343* (6174), 990−994.
(14) Chang, Y.; Braun, A.; Deangelis, A.; Kaneshiro, J.; Gailard, N. Effect of Thermal Treatment on the Crystallographic, Surface Energetics, and Photoelectrochemical Properties of Reactively Cosputtered Copper Tungstate for Water Splitting. *J. Phys. Chem. C* **2011**, *115* (51), 25490−25495.
(15) Yourey, J. E.; Kurtz, J. B.; Bartlett, B. M. Water Oxidation on a $CuWO_4$−WO_3 Composite Electrode in the Presence of $[Fe(CN)_6]^{3-}$: Toward Solar Z-Scheme Water Splitting at Zero Bias. *J. Phys. Chem. C* **2012**, *116* (4), 3200−3205.
(16) Yourey, J. E.; Pyper, K. J.; Kurtz, J. B.; Bartlett, B. M. Chemical Stability of $CuWO_4$ for Photoelectrochemical Water Oxidation. *J. Phys. Chem. C* **2013**, *117* (17), 8708−8718.
(17) Nam, K. M.; Park, J. T. Chemical Approach to a New Crystal Structure: Phase Control of Manganese Oxide on a Carbon Sphere Template. *Chem. - Asian J.* **2014**, *9* (12), 3525−3532.
(18) Patterson, A. L. The Scherrer Formula for X-Ray Particle Size Determination. *Phys. Rev.* **1939**, *56*, 978−982.
(19) Zheng, J. Y.; Song, G.; Kim, C. W.; Kang, Y. S. Facile Preparation of p-CuO and p-CuO/n-$CuWO_4$ Junction Thin Films and Their Photoelectrochemical Properties. *Electrochim. Acta* **2012**, *69*, 340−344.
(20) Gaillard, N.; Chang, Y.; DeAngelis, A.; Higgins, S.; Braun, A. A Nanocomposite Photoelectrode Made of 2.2 eV Band Gap Copper Tungstate ($CuWO_4$) and Multi-wall Carbon Nanotubes for Solar-assisted Water Splitting. *Int. J. Hydrogen Energy* **2013**, *38* (8), 3166−3176.

DOI: 10.1021/acs.langmuir.5b01780
Langmuir 2015, 31, 10897−10903

(21) Barber, J. Photosynthetic Energy Conversion: Natural and Artificial. *Chem. Soc. Rev.* **2009**, *38*, 185−196.
(22) Robinson, D. M.; Go, Y. B.; Mui, M.; Gardner, G.; Zhang, Z.; Mastrogigiovanni, D.; Garfunkel, E.; Li, J.; Greenblatt, M.; Dismukes, G. C. Photochemical Water Oxidation by Crystalline Polymorphs of Manganese Oxides: Structural Requirements for Catalysis. *J. Am. Chem. Soc.* **2013**, *135* (9), 3494−3501.
(23) Kanan, M. W.; Surendranath, Y.; Nocera, D. G. Cobalt−phosphate oxygen-evolving compound. *Chem. Soc. Rev.* **2009**, *38*, 109−114.
(24) Jin, K.; Park, J.; Lee, J.; Yang, K. D.; Pradhan, G. K.; Sim, U.; Jeong, D.; Jang, H. L.; Park, S.; Kim, D.; Sung, N.-E.; Kim, S. h.; Han, S.; Nam, K. T. Hydrated Manganese(II) Phosphate ($Mn_3(PO_4)_2 \cdot 3H_2O$) as a Water Oxidation Catalyst. *J. Am. Chem. Soc.* **2014**, *136* (20), 7435−7443.
(25) Gamelin, D. R. Water Splitting: Catalyst or Spectator? *Nat. Chem.* **2012**, *4*, 965−967.
(26) Ye, H.; Park, H. S.; Bard, A. J. Screening of Electrocatalysts for Photoelectrochemical Water Oxidation on W-Doped $BiVO_4$ Photocatalysts by Scanning Electrochemical Microscopy. *J. Phys. Chem. C* **2011**, *115* (25), 12464−12470.
(27) Mi, Q.; Zhanaidarova, A.; Brunschwig, B. S.; Gray, H. B.; Lewis, N. S. A Quantitative Assessment of the Competition Between Water and Anion Oxidation at WO_3 Photoanodes in Acidic Aqueous Electrolytes. *Energy Environ. Sci.* **2012**, *5*, 5694−5700.
(28) Hill, J. C.; Choi, K.-S. Effect of Electrolytes on the Selectivity and Stability of n-type WO_3 Photoelectrodes for Use in Solar Water Oxidation. *J. Phys. Chem. C* **2012**, *116* (14), 7612−7620.
(29) Seabold, J.; Choi, K.-S. Effect of a Cobalt-Based Oxygen Evolution Catalyst on the Stability and the Selectivity of Photo-Oxidation Reactions of a WO_3 Photoanode. *Chem. Mater.* **2011**, *23* (5), 1105−1112.

DOI: 10.1021/acs.langmuir.5b01780
Langmuir 2015, 31, 10897−10903